H. Derakhshan, Y. Nakamura, M. C. Griffith & J. M. Ingham
Suitability of height amplification factors for seismic assessment of existing unreinforced masonry components
Journal of Earthquake Engineering, 2020; OnlinePubl:1-20

Acceleration amplification factor for seismic assessment of existing non-structural unreinforced masonry components

Derakhshan, H[1], Nakamura, Y[2], Griffith, M.C[3,4], Ingham, J.M[5]

[1] Queensland University of Technology, QLD, Australia

[2] Senior Structural Engineer, WSP Australia Pty Limited, Adelaide, Australia

[3] University of Adelaide, SA, Australia

[4] Bushfire and Natural Hazards Cooperative Research Centre, Melbourne, Australia

[5] University of Auckland, New Zealand

ABSTRACT

The acceleration demand on non-structural unreinforced masonry (URM) components was investigated. The focus of the numerical study was on characterising the effects of diaphragm flexibility and the building inelastic response. It was identified that flexible diaphragms amplify the accelerations by up to 3 when compared to the case of the same building but with rigid diaphragms. It was also found that code-based assessment of acceleration amplification in URM buildings corresponds to an 'extensive' level of building damage and that this level of damage can be irrelevant when assessing relatively weak non-structural components. Modifications were proposed to the code formula.

INTRODUCTION

The seismic input to non-structural building components is in the form of absolute acceleration response of the main lateral-load-resisting system (LLRS). For a low-rise unreinforced masonry (URM) building, this LLRS is comprised of the in-plane loaded masonry walls and the horizontal floor/roof diaphragms. The effects of the response of each of these LLRS elements have been studied both numerically (Menon and Magenes 2011) and experimentally (e.g. Bothara et al. 2010; Beyer et al. 2015). The predominant features of the seismic input to URM components as reported in the aforementioned studies include the general reduction in the amplitude with an increase in the LLRS inelastic response and an increase in the acceleration response due to diaphragm flexibility (Lourenco et al. 2011; Derakhshan et al. 2016; Nakamura et al. 2017a). In addition, further resonance effects between the component and the LLRS have been studied by Degli Abbati et al. (2019).

Whilst the state-of-the-art estimation of the seismic input can be made using nonlinear time history analyses (NLTHA), the use of this method is impractical for a typical engineering consultancy project. Therefore, engineers mostly refer to the simplified methods that are available in seismic loading codes/guidelines, including the procedures recommended in the Australian seismic loading code, AS1170.4 (AS 2007), the New Zealand equivalent, NZ1170.5 (NZS 2004), and the American Society for Civil Engineering (ASCE/SEI) guidelines, "Seismic Evaluation and Retrofit of Existing Buildings" (ASCE 2017).

The current procedures in the above-mentioned references address wall-related modifications through the introduction of an acceleration amplification factor, i.e. Height Amplification Factor (HAF), but a shortcoming of the methods is that they exclude the diaphragm flexibility effect from their scope. Furthermore, the basis for the 'Parts' evaluation procedures in AS 1170.4 and NZS 1170.5 is the dynamic analyses conducted on medium to high-rise (3 to 20 storeys) reinforced concrete and steel buildings with a ductility ranging from 3 to 6 (Shelton 2004). Although these analyses were aimed at representing the effects of inelastic LLRS response on the seismic input to non-structural components, the properties of LLRS do not match that of URM buildings. Consistently, a subsequent NLTHA reported by Petrone et al. (2016) on multi-degree-of-freedom (MDOF) showed that the HAF provisions in various codes were conservative only if considerable inelastic response is taken into consideration. The MDOF models represented five highly-ductile RC frame structures with behaviour factors of equal or greater than 5.

In the context of URM buildings, it is currently unknown if the inelastic response of LLRS has benefits in reducing the seismic demand on URM components given that some of the components can fail while the building is relatively undamaged. In particular, these component failures can occur if flexible diaphragms amplify the ground accelerations which are inadequate to cause significant inelastic response to the in-plane loaded walls.

The reported research was developed with the goal to study the suitability of current code-based methods for calculation of the HAF relevant to non-structural URM components, and in particular the relevance of building inelastic response in reducing HAF. It was also an objective of this study to evaluate the significance of flexible floors on acceleration response amplification. Discussion is included pertaining to code-based methods for evaluation of acceleration demand, an investigation of empirical data on diaphragm flexibility effect, MDOF static and dynamic analyses that were conducted on four URM building models, an interpretation of the relationship between HAF and inelastic response including the effects of flexible diaphragms, and finally an assessment of the code provisions for some common non-structural URM components.

ACCELERATION DEMAND ON URM COMPONENTS

In order to provide a context for the simplified method described later, Equation (1) can be considered to produce the seismic demand on non-structural components. This equation is similar to that provided in the AS 1170.4 and NZS 1170.5 but additionally includes a diaphragm flexibility factor:

$$C_p = \frac{PFA.C_d.C_i}{R} \quad (1)$$

where, C_p, is the acceleration demand on a component, *PFA* is the peak floor absolute acceleration at the height of the component assuming rigid diaphragms, C_d is a diaphragm flexibility factor, C_i is a part spectral response factor, and *R* is a component response modification factor. AS (2007) recommends alternative values of 1 or 2.5 for both R and C_i depending on the behaviour of the component and its connections. For rigid components with rigid connections, the recommended values for both R and C_i are 1. More refined procedures are included in the NZS 1170.5, i.e. R-factor (represented by C_{ph} in NZS 1170.5) as a function of the component ductility and C_i as a function of the part period, T_p.

The *PFA* is implicitly represented in the aforementioned codes by a HAF times the peak ground acceleration (PGA), with HAF being obtained in the AS/NZ codes as:

$$HAF = 1 + \frac{x}{6} \quad \text{for } x<12 \text{ m } \& \text{ } h<12 \text{ m} \quad (2)$$

where x is the height from ground to the centre of the part, and h is the building total height. Equation (2) produces a maximum HAF of 3, which is associated with the roof of the buildings that are taller than 12 m. The ASCE (2017) recommends Equation (3), which unlike Equation (2) produces a roof amplification factor of 3 irrespective of the building height:

$$HAF = 1 + \frac{2x}{h} \quad (3)$$

In order to characterise diaphragm effect, C_d, related empirical data are presented in the next section followed by the results of MDOF analysis of building typologies in subsequent sections.

EMPIRICAL DATA ON DIAPHRAGM FLEXIBLITY EFFECT

Considerable empirical data are available on the response of buildings with relatively rigid walls and flexible diaphragms. The data from nine buildings (Table 1) were obtained from the Centre for Engineering Strong Motion Data (CESMD 2019) for a qualitative evaluation of the effects of diaphragm flexibility. The buildings included unreinforced brick (URBM), unreinforced concrete block (URCM), reinforced masonry (RM), and block masonry (BM) wall constructions. The building height varied from 6.7 m to 12.6 m, and the horizontal diaphragms were made of timber sheathing on timber joists and/or steel framing.

Table 1: Representative instrumented buildings from CESMD

Station No.	Reference	Material	H, m	Diaphragm	
				Length, L (m)	Length-to-width ratio, L/B
58264	Palo Alto	URBM	7.3	47	2.0
57476	Gilroy	URBM	7.9	13	1.1
24517	Lancaster	URCM	12.6	23	1.1
23495	Redlands	RM	8.8	40	1.5
47391	Hollister	RM	9.1	85	2.8
57502	Milpitas	RM	9.6	51	1.4
58235	Gym	RM	10.1	45	1.3
58348	Pleasant Hill	RM	12.4	40	1.7
89473	Fortuna	BM	6.7	68	1.1

The acceleration amplification at the top of the walls (Amp_w) and at the mid-span of the diaphragms in short direction (Amp_d) are plotted vs PGA in, respectively, Figure 1a and Figure 1b. The data correspond to, collectively, 22 building/earthquake scenarios that included a maximum building acceleration of at least 0.15g. It can be found in Figure 1a that Amp_w was mostly limited to under 2, with an overall decrease in the amplification with an increase in earthquake intensity. The data labels on Figure 1a indicate the building height, with the amplifications having no specific correlation with this parameter. This lack of correlation was attributed to the diaphragm effects which have overshadowed the effect of building height on wall accelerations. The data in Figure 1b suggests that Amp_d was up to nearly 6, with the Amp_d/Amp_w ratio (Figure 1c) varying from about 1 to more than 4. However for most cases, the ratio can be found to be limited between 1.5 and 3.5. Although a robust parametric study was impractical due to the large variability in building details, the above data provides an empirical basis for studying the acceleration amplifying effects of diaphragm flexibility.

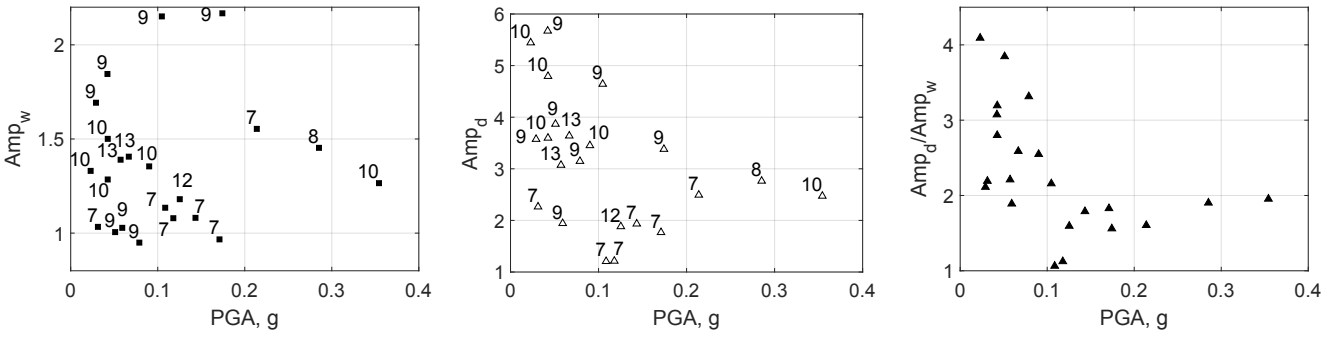

a) In-plane loaded wall top b) Diaphragm mid-span c) Diaphragm to wall ratio

Figure 1: Empirical acceleration data for buildings with flexible diaphragms; data labels refer to building heights

MDOF STUDY

An equivalent frame (EF) computer package, Tremuri (Lagomarsino et al. 2013) was used to analyse four URM building models represented by the plan dimensions shown in Figure 2. The computer program has been shown to be capable of modelling inelastic behaviour of regular masonry buildings (see Nakamura et al. 2016; Marino et al. 2019). Buildings 1-A and 1-B were one-storey with different plans and wall opening arrangements. Buildings 2 and 3 had the same plan dimensions and were, respectively, two-storey and three-storey. The storey height was assumed to be 4.25 m at the ground floor and 3.5 m in the upper floors. The ground-storey and upper-storey walls were assumed to be, respectively, 350 mm and 230 mm thick.

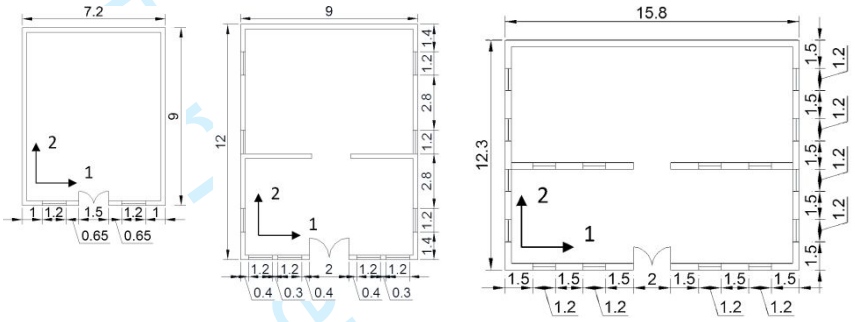

(a) Type 1-A (b) Type 1-B (c) Types 2 and 3

Figure 2: Building plans

The buildings were assumed to be made of solid, fired, clay brick units with a relatively weak lime-rich mortar representing pre-1940 URM buildings (Lumantarna 2012). Masonry density was assumed as 1900 kg/m^3 and other material properties are listed in Table 2.

Table 2. Masonry material properties

Young's modulus	Shear modulus	Compressive strength	cohesion	Friction coefficient
1385 MPa	740 MPa	5.74 MPa	0.130 MPa	0.111

The default modelling procedure in the software provides the possibility for partial or full 'coupling' between the in-plane loaded walls through the introduction of diaphragm stiffness properties. However, a diaphragm mass DOF that enables modelling its vibrations requires a 'manual' procedure of overwriting mass assignments. The procedure includes the definition of additional DOF at diaphragm(s) mid-span(s) and has been validated in Nakamura et al. (2017a; 2017b) and used in this research.

Diaphragm in-plane stiffness was introduced as a variable in a parametric study framework. Default material properties for existing timber floors have been recommended in (ASCE 2014) in the form of a characteristic shear stiffness, G_d, with a minimum value of 350 kN/m. Further in-situ testing of URM buildings in New Zealand has suggested values (Giongo et al. 2014) up to a third of this stiffness depending on the

condition (e.g. decay in timber joists) of the diaphragm. To accommodate these recommendations, a lower bound G_d=150 kN/m (designated as D1) was used along with 4 other greater diaphragm stiffness properties (Table 3). These properties include a strengthened (D4) and a theoretically rigid diaphragm (D5).

Table 3: Range of diaphragm stiffness properties

Designation	Description	G_d, kN/m	T_d*
D1	As-built with single straight sheathing	150	1.08
D2	As-built with single diagonal sheathing; unchorded	600	0.54
D3	As-built with double straight sheathing; chorded	2400	0.27
D4	Single straight sheathing strengthened with 19 mm plywood overlay with substantial edge nailing	9600	0.13
D5	Large stiffness representing a rigid diaphragm	3 x 10^6	0.01

* Calculated using the diaphragm stiffness and the combined mass of the diaphragm and the tributary mass of the out-of-plane loaded walls (small variations for different buildings ignored)

Diaphragm loads were assumed to represent a commercial/governmental office building with floor live dead and seismic weight reduction factor of respectively, 3 kPa and 0.4. A reference trussed roof dead load of 1.5 kPa was calculated assuming 0.7 kPa from roof trusses in addition to 0.8 kPa from secondary members and concrete tiles. A floor dead load of 1.0 kPa was assumed including 0.45 kPa for a lath and plaster ceiling.

Pushover analyses

Pushover analyses were completed to obtain behavioural data (Figure 3a to Figure 3d), which assist in the calculation of HAF corresponding to building damage states (DS). Cyclic displacements were prescribed in the symmetric direction of the buildings, with the 'control node' being placed on the roof level. The lateral load pattern was assumed to be mass-proportional-linear to obtain a conservative estimate of the roof displacement (Nakamura et al. 2017b; Endo et al. 2017). The admissibility of the pushover results was checked at the end of analysis by evaluating the net vertical reactions at the wall bases against the total building weight.

An idealised bilinear elastic-perfectly-plastic (EPP) model (Figure 3e) was fitted to the curves to calculate the idealised elastic (De) and ultimate inter-storey drifts (Du), with the results being reported in Table 4. Building 2 underwent rocking displacements, and therefore the ultimate building drift was assumed to be 1.3%.

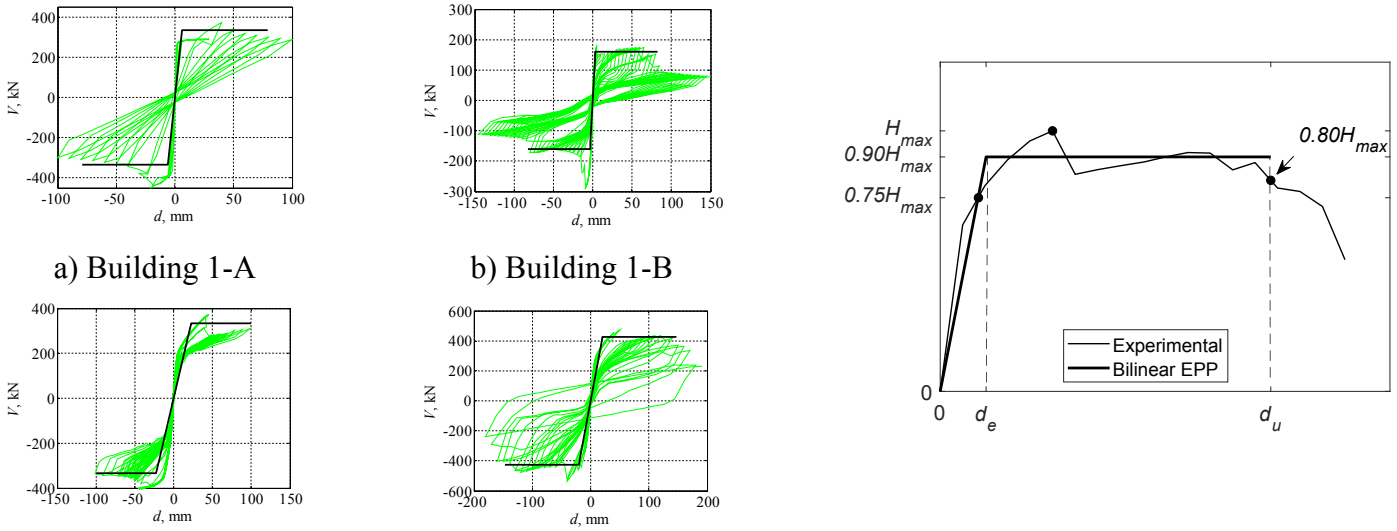

Figure 3: Pushover curve and bilinear idealisation

In order to make an interpretation of acceleration response with respect to qualitative building damage, drift limits corresponding to four damage states were determined using D_e and D_u and following Lagomarsino and Cattari (2014). These damage states are: Slight (D1), Moderate (D2), Extensive (D3), and Collapse (D4), with the associated drift thresholds being listed in Table 4. The drift threshold data were found to be comparable to the lower bound of the ranges suggested by D'Ayala et al. (2014) based on a literature review of tests on stone and brick masonry construction with lime mortar. The values were also found to be consistent with Lagomarsino and Cattari (2014) and with low-code/pre-code values from Hazard-US Multi-hazard program (HAZUS; FEMA 2012). Table 4 also includes the first mode period of the buildings calculated from modal analysis.

Incremental dynamic analyses

Incremental dynamic analysis (IDA) was conducted to obtain two measures of earthquake intensity, i.e. PGA and $S_a(T_1)$ corresponding to each DS. For this purpose, a suite of 6 real Normal or Strike-Slip, shallow, earthquake records with M_w ranging from 5.9 to 6.6 were used, with the acceleration time histories being recorded mostly on shallow or narrow deep soils. The spectral acceleration of the records has been shown in Figure 4, overlapped with bold dashed lines that were fitted to calculate corner periods, T_o and T_c, and a mid-point, T'_s, that approximately corresponds to peak average spectral acceleration. Rayleigh viscous damping was used with a 5% initial damping ratio assigned at two (lower and higher) frequencies corresponding to, respectively, the fundamental mode ($1/T_1$) and the lowest elastic mode containing 90% mass participation.

Table 4. Building behavioural data

Model	D_e[1], %	D_u[2], %	DS1[3], %	DS2[4], %	DS3[5], %	DS4[6], %	T_1[7], sec
1-A	0.14	1.86	0.11	0.71	1.29	1.86	0.06
1-B	0.07	1.93	0.05	0.35	1.18	1.93	0.10
2	0.30	1.30	0.38	1.00	2.00	2.70	0.25

Model	D_e[1], %	D_u[2], %	DS1[3], %	DS2[4], %	DS3[5], %	DS4[6], %	T_1[7], sec
3	0.18	1.30	0.15	0.50	0.90	2.50	0.38; 0.15

1: bilinear elastic drift; 2: bilinear ultimate drift limit; 3: slight damage state; 4: moderate damage state; 5: extensive damage state; 6: collapse 7: first mode period from modal analysis

The IDA curves are shown in Figure 5 and Figure 6 for excitations in both directions of the buildings. These plots also include threshold drift data (horizontal dash lines), which were used to calculate the median earthquake intensities associated with DSs. These quantities (Table 5) were estimated from the IDA curves as the smallest intensity in any loading direction at which 50% of the records cause respective inter-storey drift thresholds. Due to the pushover analyses being conducted only on the symmetric direction, the drift limits for asymmetric direction (Direction 1) was averaged from that for the symmetric directions.

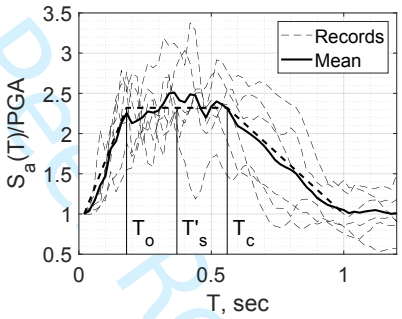

Figure 4: Spectral acceleration of the earthquake records

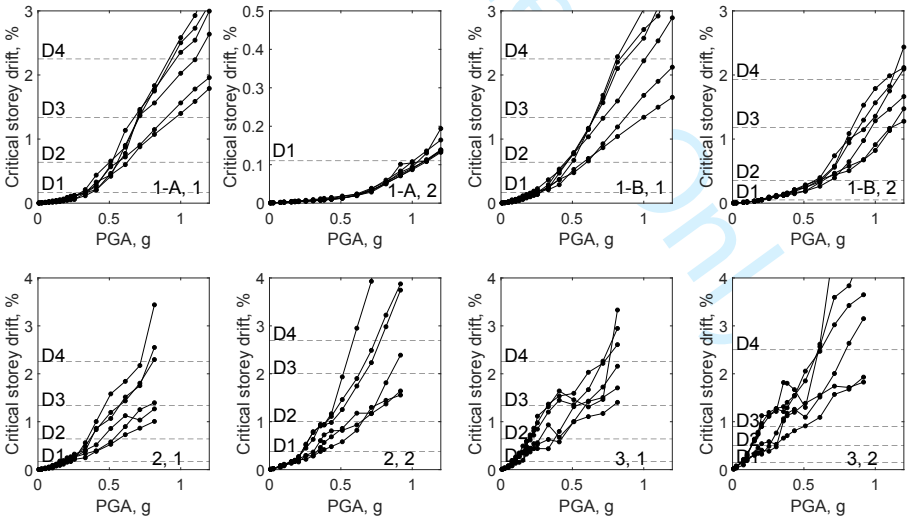

Figure 5: IDA curves; critical inter-storey drift vs. PGA

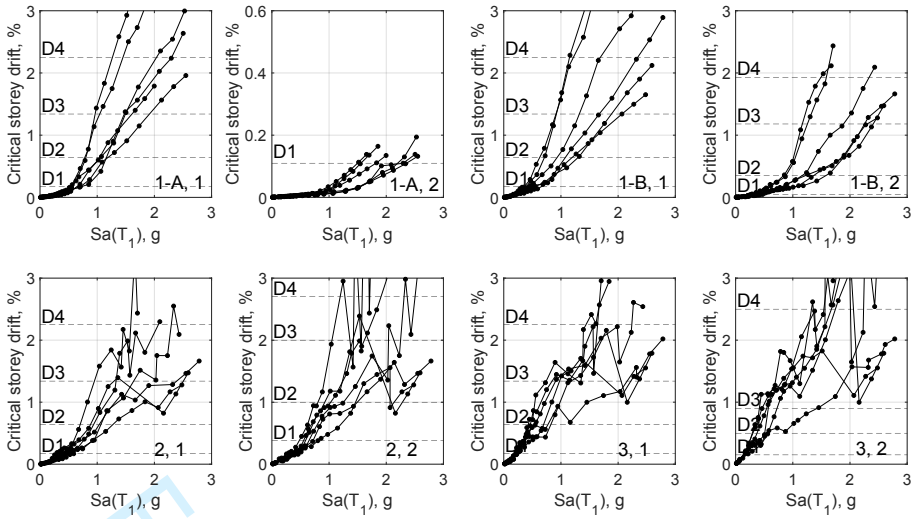

Figure 6: IDA curves; critical inter-storey drift vs. spectral acceleration

CALCULATED BUILDING RESPONSE

In Figure 7 the response acceleration data is plotted for shaking in the symmetric direction (Direction 2) vs. T_d/T'_s, with T_d and T'_s being defined in, respectively, Table 3 and Figure 4. For buildings with T_1 smaller than T_o (0.18 sec), i.e. Buildings 1-A (T_1=0.06 sec) and 1-B (T_1=0.10 sec), an increase in diaphragm flexibility has led to increased acceleration amplification with the peak occurring near T_d/T'_s=1. The maximum amplification is between 2.1 and 3.0 times that occurring for the case of rigid diaphragms, i.e. T_d/T'_s approaching to zero (see top 2 sub-plots in Figure 7a). The upper and lower bounds of this ratio are associated with, respectively, the smallest and the largest applied accelerations.

Table 5: Limits of earthquake intensity measures for damage states

DS	DS1 (slight)		DS2 (moderate)		DS3 (extensive)		DS4 (collapse)	
Building	PGA, g	$S_a(T_1)$, g	PGA, g	$S_a(T_1)$, g	PGA, g	$S_a(T_1)$, g	PGA, g	$S_a(T_1)$, g
Average (1-A&1-B)	0.27	0.58	0.51	0.99	0.69	1.39	0.92	1.87
2	0.17	0.39	0.37	0.94	0.57	1.47	0.78	2.22
3	0.06	0.15	0.13	0.37	0.20	0.54	0.62	1.46
Average	0.17	0.56	0.34	0.77	0.49	1.13	0.77	1.85

The initial increase in amplification with an increase in diaphragm period is due to T_d approaching to or falling in the range of the response spectra plateau and therefore imparting a greater spectral acceleration in the building response. Conversely, there is a decrease in amplification for larger T_d/T'_s ratios due to reduction in the spectral response associated with the diaphragm.

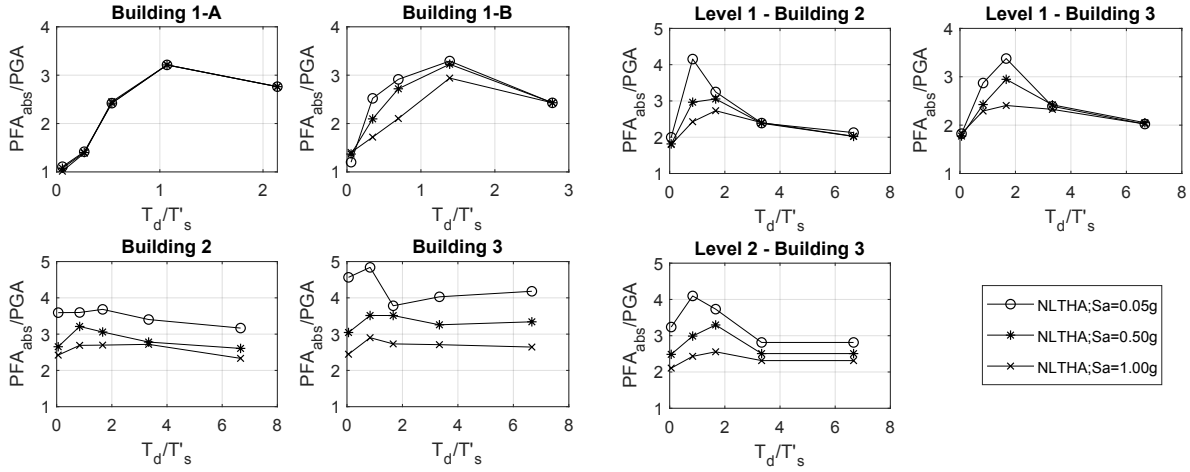

a) Roof level b) Floor levels

Figure 7: Acceleration amplification in buildings with flexible diaphragms

In contrast, the roof acceleration amplification for Buildings 2 (T_1=0.25) and 3 (T_1=0.38) mostly reduced or remained constant (see bottom 2 sub-plots in Figure 7a) with an increase in diaphragm flexibility. This pattern is attributed to the building already responding with near-peak spectral acceleration in the rigid diaphragm case, and an increase in the diaphragm period resulting in some building mass being mobilised with a period greater than T_c and a smaller modal acceleration response.

For the lower floors of Buildings 2 and 3 (Figure 7b), the amplifying effects of diaphragm flexibility are significant. The reason for this amplification is the smaller ordinate of the global building mode shape at lower floors when the diaphragms are rigid. Increasing diaphragm flexibility promotes new localised modes that can be associated with near peak spectral acceleration, hence amplifying the otherwise smaller wall-related accelerations.

The above-mentioned diaphragm-related amplification range of between 1 and 3 for building roofs is consistent with the range of 1.5 to 3.5 that was found for the ratio of flexible diaphragm acceleration to wall acceleration in the same building from the empirical data.

COMPARISON WITH SEISMIC LOADING CODES

In order to be able to provide recommendation on the effects of diaphragm flexibility from a practical perspective, e.g. by using a C_d for use with Equation (1), the calculated response in Figure 7 was compared to code-based values for buildings with rigid diaphragms. This comparison is made in Table 6 between HAF for the worst case scenario of diaphragm flexibility effect calculated from Figure 7 and the HAF from Equations (2) and (3). The comparisons are made for several levels of earthquake intensity including that corresponding to various DSs.

Table 6: Ratio (C_d) of HAF including the worst case diaphragm effect to code-based calculations

DS	Building	1-A & 1-B	2		3			
	Ratio	x=4.25m	x=4.25m	x=7.75m	x=4.25m	x=7.75m	x=11.25m	Average (CV)
PGA= 0.0075g	to Eq. (2)	1.9	2.4	1.6	2.0	1.8	1.7	1.9 (0.15)
	to Eq. (3)	1.1	2.0	1.2	1.9	1.7	1.6	1.6 (0.22)
DS1	to Eq. (2)	1.9	1.9	1.5	1.9	1.6	1.6	1.7 (0.12)
	to Eq. (3)	1.1	1.5	1.1	1.8	1.5	1.5	1.4 (0.19)
DS2	to Eq. (2)	1.8	1.6	1.2	1.8	1.5	1.3	1.5 (0.17)
	to Eq. (3)	1.0	1.3	0.9	1.7	1.4	1.3	1.3 (0.23)
DS3	to Eq. (2)				1.7	1.4	1.2	1.4 (0.17)
	to Eq. (3)				1.6	1.4	1.2	1.4 (0.16)
Average	to Eq. (2)							1.6
	to Eq. (3)							1.4

It can be found from Table 6 that the ratios of HAF including the worst case diaphragm effect to code-based calculations (C_d) decrease with an increase in building damage, and that these ratios are generally larger in the lower storeys. The reason for the more prominent effect in the lower storeys was previously discussed and is due to the more pronounced diaphragm accelerations when compared to the wall accelerations.

The individual C_d ratios can be as high as 2.4, e.g. for PGA=0.0075g, x=4.25 m, and Building 2 if AS/NZ code is used. However smaller values are obtained corresponding to ASCE (2017) code and/or larger shaking. The average C_d ratio from all floor levels is detailed in the last column of Table 6 and reduces from 1.9 (PGA=0.0075g) to 1.4 (DS3) for the calculations that were made using AS/NZ codes (Equation 2). The value ranges from 1.6 (PGA=0.0075g) to 1.3 (DS2) for the calculations that were made using ASCE guidelines (Equation 3; see the shaded cells in the last column of Table 6). With reference to the average values, it is considered appropriate to assume a C_d=1.6 in conjunction with ASCE (2017) to address diaphragm flexibility effects. The ratio is mostly conservative, except for the ground floor and where the building responses are close to elastic.

Specific case of rigid diaphragms

The average HAFs from the 6 applied records are plotted in Figure 8 for the rigid diaphragm case, with the plots being overlapped with vertical dashed lines representing DS thresholds. The ratio of code-based HAF from Equations (2) and (3) to the numerical calculations are detailed in Table 7. It can be found from Table 7 that both the ASCE and AS/NZ codes grossly overestimate (by between 50% and 190%) the amplification factor for one-storey buildings. This overestimation is attributed to 1) the buildings being practically rigid, i.e. T_1<0.10sec, and therefore having an insignificant relative acceleration; and 2) the code-based formula

includes an algebraic sum of PGA and maximum relative acceleration, with this calculation having a tendency to overestimate the actual response.

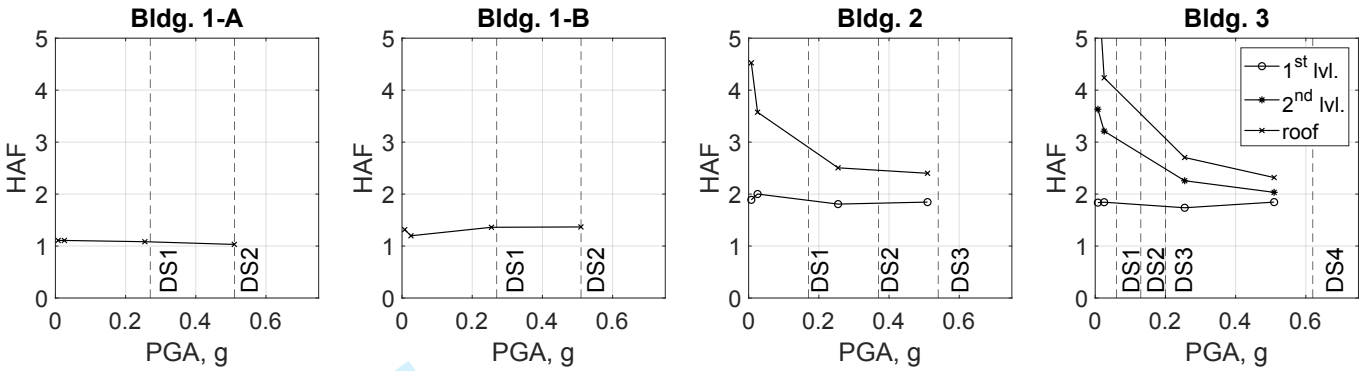

Figure 8: Acceleration amplification vs PGA

For two-storey and three-storey buildings, it can be found that both codes are conservative for a building damage state of DS3. For DS2, both codes are non-conservative for the three-storey building, and in addition the AS/NZ code is non-conservative for the two-storey building. For close to elastic behaviour none of the codes are conservative except when applied to single-storey buildings.

Table 7: Ratio of code-based HAF to MDOF calculations

DS	Building	1-A and 1-B	2		3		
	Elevation	x=4.25m	x=4.25m	x=7.75m	x=4.25m	x=7.75m	x=11.25m
PGA= 0.0075g	AS/NZ	1.6	0.9	0.6	0.9	0.7	0.6
	ASCE	2.9	1.1	0.8	1.0	0.7	0.7
DS1	AS/NZ	1.5	0.9	0.8	0.9	0.7	0.7
	ASCE	2.6	1.1	1.0	1.0	0.8	0.7
DS2	AS/NZ	1.5	0.9	1.0	0.9	0.9	0.8
	ASCE	2.6	1.2	1.3	1.0	0.9	0.9
DS3	AS/NZ				1.0	1.0	1.0
	ASCE				1.0	1.0	1.0

Overall from the above discussion it can be concluded that for the relatively small ground accelerations of interest, the ASCE (2017) provides a better estimate of acceleration amplification. In particular, calculation using Equation (3) can be multiplied by a coefficient C_d to include diaphragm-related amplifications at building roofs irrespective of the building height.

AMPLIFICATION FACTOR FOR URM COMPONENTS

As discussed in the previous section, code-based HAF can be non-conservative if the LLRS is expected to have close to elastic behavior, and therefore a methodology is proposed here to include varying degrees of

LLRS inelastic response effect depending on the component strength. For this purpose, the data in Figure 8 is re-plotted in the form of HAF versus the seismic demand on components (HAF.PGA=PFA) assuming rigid diaphragm. This relationship has been shown as solid lines in Figure 9a for the three-storey building. Equation (1) is next re-formulated to obtain the PFA corresponding to component failure, $\widehat{PFA}$, as a function of the component strength and other amplifying factors:

$$\widehat{PFA} = \frac{a_u.R}{C_d.C_i} \quad (4)$$

Because all of the parameters on the right side of Equation (4) are known for an existing component, $\widehat{PFA}$ can be calculated and used to estimate HAF from Figure 9a. Using this method, it can be found from Figure 9a that HAF increases with a reduction in the component strength. To develop a generic formula, Equations (2) and (3) can be modified to capture this increase in the HAF. As discussed earlier, the HAF calculated from Equations (2) and (3) matched or reasonably overestimated the HAF from MDOF models corresponding to DS3. This damage state is associated with a PFA of 0.6g in the three-storey building. Using a PFA of 0.6g as a benchmark, Equation (2) is modified as Equation (5):

$$HAF = 1 + \frac{x}{6}(1.6 - \widehat{PFA}) \quad \text{for } \widehat{PFA} \leq 0.6 \quad (5)$$

$$HAF = 1 + \frac{x}{6} \quad \text{for } \widehat{PFA} > 0.6$$

which has the same validity as for Equation (2), i.e. for h<12 m. Similarly, Equation (3) is modified as:

$$HAF = 1 + \frac{2x}{h}(1.6 - \widehat{PFA}) \quad \text{for } \widehat{PFA} \leq 0.6 \quad (6)$$

$$HAF = 1 + \frac{2x}{h} \quad \text{for } \widehat{PFA} > 0.6$$

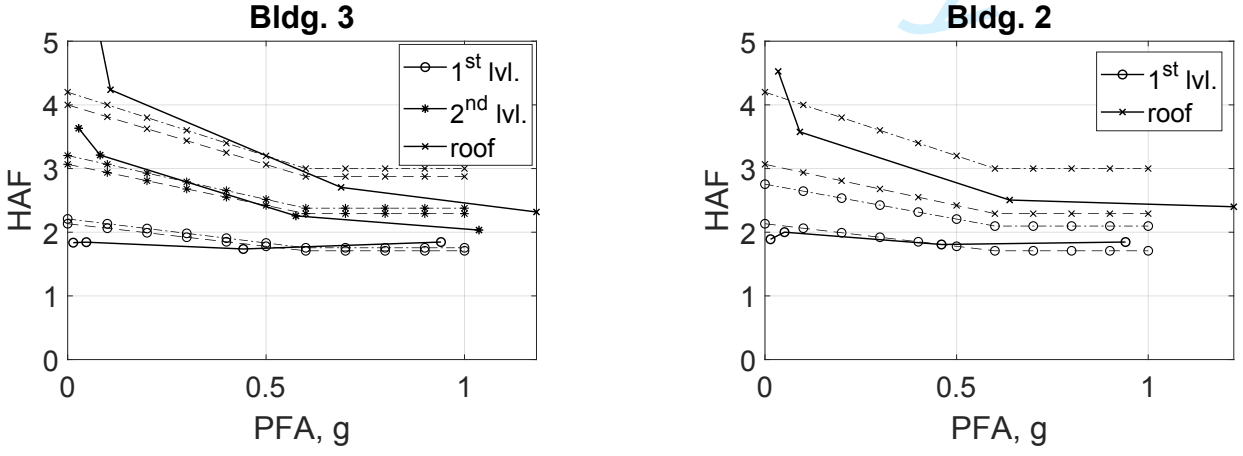

a) Building 3 b) Building 2

Figure 9: HAF versus acceleration demand for a building with rigid diaphragm

In Figure 9a the HAF from Equations (5) and (6) have been plotted versus PFA by, respectively, dashed and dash-dotted lines. In Figure 9b the same data were used for the two-storey building, which shows that the calculations using Equation (6), being the dash-dotted lines, can adequately capture the increase in HAF with reduction in the demand. Therefore, Equation (6) is recommended to be used for the calculation of HAF in URM buildings.

Case study, roof-top URM cantilevers

Equations (6) is used to obtain estimates of HAF for URM chimneys and parapets. Three lateral load tests on URM chimneys were reported in Derakhshan et al. 2018a, with the study suggesting that the measured peak strength correlated well with Equation (7):

$$a_u = \frac{b}{h_p} \quad (7)$$

where a_u is the equivalent lateral acceleration in 'g' units required for the onset of overturning, b is chimney width, and h_p is its height. The same equation can be assumed appropriate for older URM parapets, which are often built on a damp-proof-membrane (Doherty 2002).

Calculations were made using Equation (7) to obtain a_u for median geometries of chimneys and parapets. The chimney and parapet geometries were assumed based on, respectively, Derakhshan et al. (2018a) and Walsh et al. (2014) as detailed in Table 8. Using Equation (7), a_u for these components can be obtained as, respectively, 0.24g and 0.17g. Assuming a C_d of 1.6 based on the previous discussions, a response modification factor of 1, and a part spectral acceleration factor of 1 based on AS (2007), $\widehat{PFA}$ is obtained from Equation (4) as, respectively, 0.15g and 0.11g. Using these values, the amplification factor is calculated using Equation (6) as approximately 4.0 for the parapet and approximately 3.9 for the chimney as detailed in Table 8. These values have good correlation with the MDOF results, also included in Table 8.

Table 8: Case studies of calculating height amplification factor

Component	x	h	b	hp	a_u	R	C_d	C_i	$\widehat{PFA}$	HAF		
	m	m	mm	mm	g				g	Eq. 3	MDOF**	Eq. 6
Parapet	11.25	11.25	230	1390	0.17	1	1.6	1	0.11	3	4.2	4.0
Chimney	11.25	11.25	470	1930	0.24	1	1.6	1	0.15	3	4.1	3.9
Two-way spanning walls	9.50*	11.25	---	---	0.60	2.5	1.6	2.5	0.38	2.7	3.1	3.1
Plastered two-way spanning	9.50*	11.25	---	---	1.30	2.5	1.6	2.5	0.81	2.7	2.4	2.7

* Corresponding to wall centre; ** Mid-point between solid lines corresponding to 2nd level and roof in Figure 9a

Case study, two-way spanning out-of-plane loaded walls

The mean strength of 8 two-way spanning walls reported in Derakhshan et al (2018b) were used to estimate the appropriate HAFs for these components. The average wall strength, a_u, was recorded as 1.3g and 0.6g, respectively, for walls with and without plaster on the tension surface. Both R-factor and C_i were assumed as 2.5 based on AS 1170.4 recognising the relative flexibility and ductility of the two-way spanning walls. The calculations as summarised in Table 8 suggest that $\widehat{PFA}$ for walls without plaster located at the top-storey of the three-storey building is smaller than 0.6g, and therefore the modifications suggested in Equation (6) will apply to these components. Using Equation (6), the amplification factor is obtained as 3.1, which is larger than that obtained from Equation 3 (2.7).

In contrast, the $\widehat{PFA}$ of 0.81g for walls with plaster located at the top-storey of the three-storey building is greater than 0.6g. Therefore, the amplification factor for these walls is not affected by the modifications presented in Equation (6), and code-based formula, e.g. Equation (3) can be used to calculate HAF.

In summary from these case-studies, it can be concluded that for existing two-way spanning walls without plaster or for existing URM cantilevers, a larger amplification factor than that prescribed in seismic loading codes should be used. For an existing component with a known strength, i.e. a_u, Equations (4) and (6) can be used in order to calculate, respectively, $\widehat{PFA}$ and the acceleration amplification.

SUMMARY AND CONCLUSIONS

Incremental dynamic analyses were conducted on MDOF models of four building typologies to characterise acceleration amplification within the buildings for a range of horizontal diaphragm stiffness properties and applied acceleration intensities. It was found that increased applied acceleration intensity generally reduces amplifications and interpretation was made on how the beneficial effects of inelastic behaviour of the primary lateral load resisting system should be taken into consideration when assessing the acceleration input to URM components.

The results were compared to code-specified values, and it was found that the codes are conservative for single-storey buildings but non-conservative for the roof-level of two or three-storey buildings. From MDOF results for each specific building/floor of interest it was found that the accelerations in buildings with flexible diaphragms are amplified by up to 3 when compared to the case of buildings with rigid diaphragms. The responses of the buildings with flexible diaphragms were compared to the code-based formula and it was found that the effects of diaphragm flexibility at the upper levels of the buildings can be adequately included using an acceleration amplifying coefficient of C_d=1.6.

It was also found that code-based values correspond to a degree of main LLRS damage that can be irrelevant when assessing relatively weaker existing URM components, i.e. URM cantilevers or two-way spanning walls without plaster, but the included LLRS damage may be appropriate for assessing two-way spanning walls that have applied plaster. A modification to two code-based formula (AS/NZ and ASCE) was made to calculate the seismic demand on components, with the formulation depending on the component strength. This methodology, which included the use of diaphragm-related coefficient, C_d, was found to produce more consistent results if applied to the ASCE formula. Case studies on existing URM components showed that roof-top URM cantilevers in a three-storey building should be assessed using a HAF of up to 4.2, as opposed to a value of approximately 3 as is recommended by seismic loading codes. Similarly, top-storey two-way spanning walls without plaster should be assessed using a greater amplification factor than that obtained from the codes. On the contrary, the code-based values were found to be appropriate for the assessment of some stronger URM components, e.g. the out-of-plane loaded two-way spanning walls with plaster on both sides. A formula was proposed that can be used to calculate the increased amplification factors for existing URM components.

ACKNOWLEDGEMENTS

The first author acknowledges the support of Australian Government through Australian Research Council Early Career Researcher Award (DE180101593). The authors gratefully acknowledge the financial support of the Australian Research Council through its Cooperative Research Centre (CRC) programme and specifically the Bushfire and Natural Hazards CRC. The views and opinions expressed in this paper are those of the authors and not necessarily those of the sponsors.

REFERENCES

AS [Australian Standards] (2007). "AS 1170.4 – Structural Design Actions Part 4: Earthquake actions in Australia", Sydney, Australia: Standards Australia.

ASCE [American Society for Civil Engineering] (2014). "ASCE 41-13: Seismic Evaluation and Retrofit of Existing Buildings", American Society of Civil Engineers, Reston, Virginia.

Beyer, K., Tondelli, M., Petry, S., and Peloso, S. (2015). "Dynamic testing of a four-storey building with reinforced concrete and unreinforced masonry walls: prediction, test results and data set". Bull Earthquake Eng (2015) 13:3015–3064. DOI 10.1007/s10518-015-9752-z.

Bothara, J. K., Dhakal, R. P., and Mander, J. B. (2010). "Seismic performance of an unreinforced masonry building: An experimental investigation". Earthquake Engineering and Structural Dynamics, 39, pp. 45-68.

CESMD [Center for Engineering Strong-Motion Data] (2019). https://strongmotioncenter.org/.

D'Ayala, D., Meslem, A., Vamvatsikos, D., Porter, K., Rossetto, T., Crowley, H., Silva, V. (2014). Guidelines for analytical vulnerability assessment of low/mid-rise buildings - Methodology, Vulnerability Global Component project. Available from: www.nexus.globalquakemodel.org/gem-vulnerability/posts/

Degli Abbati, S., Cattari, S., Lagomarsino, S. (2019). "Seismic assessment of single-block rocking elements in masonry structures". Masonry International. 31(2), pp. 39-48.

Derakhshan, H., Griffith, M.C., Ingham, J.M. (2016). "Out-of-plane seismic response of vertically spanning URM walls connected to flexible diaphragms". Earthquake Engineering and Structural Dynamics, 45(4), pp. 563-580.

Derakhshan, H., Lucas, W.D., Griffith, M.C. (2018a). "In-situ seismic verification of non-structural components of unreinforced masonry buildings", Australian Journal of Structural Engineering, 19(1), pp. 44-58.

Derakhshan, H., Lucas, W., Visintin, P., Griffith, M.C. (2018b). "Out-of-plane strength of existing two-way spanning solid and cavity unreinforced masonry walls". Structures, 13, pp. 88-101.

Doherty, K. T. (2000). "An investigation of the weak links in the seismic load path of unreinforced masonry buildings", Ph.D. Thesis, Department of Civil, Environmental, and Mining Engineering, University of Adelaide, Adelaide, SA, Australia.

Endo, Y., Pelà, L., and Roca, P. (2017). "Review of different pushover analysis methods applied to masonry buildings and comparison with nonlinear dynamic analysis". Journal of Earthquake Engineering, 21 (8), 1234-1255, DOI: 10.1080/13632469.2016.1210055.

FEMA (2012). Multi-hazard loss estimation methodology, earthquake model: HAZUS-MH 2.1, technical and user's manual, Federal Emergency Management Agency, Washington, DC.

Giongo, I., Wilson, A., Dizhur, D., Derakhshan, H., Tomasi, R., Griffith, M. C., Quenneville, P., and Ingham, J. M. (2014). Detailed seismic assessment and improvement procedure for vintage flexible timber diaphragms. Bulletin of the New Zealand Society for Earthquake Engineering, 47(2), 97-118.

Giresini, L., Sassu, M., and Sorrentino, L. (2018). "In situ free-vibration tests on unrestrained and restrained rocking masonry walls". Earthquake Engineering & Structural Dynamics. DOI: 10.1002/eqe.3119.

Griffith, M.C. and Vaculik, J. (2007). "Out-of-Plane flexural strength of unreinforced clay brick masonry walls", The Masonry Society Journal, 25(1), 53-68.

Lagomarsino, S., Penna, A., Galasco, A. and Cattari, S. (2013) "TREMURI program: an equivalent frame model for the nonlinear seismic analysis of masonry buildings," Engineering Structures, 56, 1787 – 1799.

Lagomarsino S and Cattari S (2014) "Fragility functions of masonry buildings", (Chapter 5), pp. 111-156, SYNER-G: Typology Definition and Fragility Functions for Physical Elements at Seismic Risk, Volume 27 (Eds: K. Pitilakis, H. Crowley, A.M. Kaynia), pp. 420. Springer Science+Business Media Dordrecht, doi 10.1007/978-94-007-7872-6_5

Lourenço, P.B., Mendes, N., Ramos, L.F., Oliveira, D.V. (2011). "Analysis of masonry structures without box behaviour", International Journal of Architectural Heritage, 5(4-5), pp. 369-382.

Lumantarna, R. (2012). "Material characterisation of New Zealand's clay brick unreinforced masonry buildings". PhD thesis, Department of Civil and Environmental Engineering, University of Auckland.

Marino, S., Cattari, S., Lagomarsino, S., Dizhur, D., Ingham, J.M. (2019) 'Post-earthquake damage simulation of two colonial unreinforced clay brick masonry buildings using the equivalent frame approach', Structures, 19, 212- 226. https://doi.org/10.1016/j.istruc.2019.01.010.

Menon, A. and Magenes, G. (2011). Definition of Seismic Input for Out-of-Plane Response of Masonry Walls: II. Formulation. Journal of Earthquake Engineering, 15(2): 195-213.

Nakamura, Y., Derakhshan, H., Sheikh, A.H., Ingham, J.M., and Griffith, M.C. (2016). "Equivalent frame modelling of an unreinforced masonry building with flexible diaphragms – a case study". Bulletin of the New Zealand Society for Earthquake Engineering, 49(3), 234-244.

Nakamura, Y., Derakhshan, H., Griffith, M., Magenes, G., Sheikh, A. (2017a). "Applicability of nonlinear static procedures for low-rise unreinforced masonry buildings with flexible diaphragms", Engineering structures, 137, pp 1-18; doi: 10.1016/j.engstruct.2017.01.049.

Nakamura, Y., Derakhshan, H., Magenes, G., Griffith, M., (2017b). "Influence of diaphragm flexibility on seismic response of unreinforced masonry buildings". Journal of Earthquake Engineering, 21(6), pp 935-960. doi: 10.1080/13632469.2016.1190799.

NZS [New Zealand Standards]. (2004). NZS 1170.5: Structural Design Actions: Part 5: Earthquake actions, New Zealand.

Oliver, S. (2010). "A design methodology for the assessment and retrofit of flexible diaphragms in unreinforced masonry buildings". Journal of the Structural Engineering Society New Zealand Inc. 23(1), pp. 19-49.

Penna, A., Lagomarsino, S. and Galasco, A. (2014) "A nonlinear macroement model for the seismic analysis of masonry buildings," Earthquake Engineering and Structural Dynamics, 43(2), 159 – 179.

Petrone C., Magliulo, G., Manfredi, G., "Floor response spectra in RC frame structures designed according to Eurocode 8". Bulletin of Earthquake Engineering (2016) 14:747–767.

Rota M, Penna A, Magenes G (2010) "A methodology for deriving analytical fragility curves for masonry buildings based on stochastic nonlinear analyses." Eng Struct 32:1312–1323.

Shelton, R.H. (2004), Seismic response of building parts and non-structural components. Study report, No. 124. BRANZ, Porirua City 5381, New Zealand. ISSN: 0113-3675.

Walsh, K. Q., Dizhur, D. Y., Almesfer, N., Cummuskey, P. A., Cousins, J., Derakhshan, H, Griffith, M. C., and Ingham, J. M. (2014). "Geometric characterisation and out-of-plane seismic stability of low-rise unreinforced brick masonry buildings in Auckland, New Zealand". Bulletin of the New Zealand Society for Earthquake Engineering, 47(2), June, 139-156.